Intense sub-terahertz radiation from wide-bandgap semiconductor based large-aperture photoconductive antennas pumped by UV lasers

Article *in* New Journal of Physics · October 2019

DOI: 10.1088/1367-2630/ab532e

CITATIONS
7

READS
193

9 authors, including:

Xavier Ropagnol
Institut National de la Recherche Scientifique
61 PUBLICATIONS **690** CITATIONS
SEE PROFILE

Zsolt Kovács
Magyar Tudományos Akadémia Wigner Fizikai Kutatóközpont
8 PUBLICATIONS **29** CITATIONS
SEE PROFILE

Barnabás Gilicze
13 PUBLICATIONS **47** CITATIONS
SEE PROFILE

Mariia Zhuldybina
École de Technologie Supérieure
11 PUBLICATIONS **21** CITATIONS
SEE PROFILE

PAPER • OPEN ACCESS

Intense sub-terahertz radiation from wide-bandgap semiconductor based large-aperture photoconductive antennas pumped by UV lasers

To cite this article: X Ropagnol *et al* 2019 *New J. Phys.* **21** 113042

New Journal of Physics
The open access journal at the forefront of physics

Deutsche Physikalische Gesellschaft DPG
IOP Institute of Physics

Published in partnership with: Deutsche Physikalische Gesellschaft and the Institute of Physics

OPEN ACCESS

RECEIVED
13 August 2019

REVISED
8 October 2019

ACCEPTED FOR PUBLICATION
31 October 2019

PUBLISHED
20 November 2019

PAPER

Intense sub-terahertz radiation from wide-bandgap semiconductor based large-aperture photoconductive antennas pumped by UV lasers

X Ropagnol[1,2], Zs Kovács[3,4], B Gilicze[3], M Zhuldybina[2], F Blanchard[2], C M Garcia-Rosas[1], S Szatmári[3], I B Földes[3,4] and T Ozaki[1]

[1] INRS-EMT, 1650 Boulevard Lionel Boulet, Varennes, Québec, Canada
[2] Department of Electrical Engineering/ ÉTS, 1100 rue Notre-Dame Ouest, Montréal, Québec, Canada
[3] Department of Experimental Physics, University of Szeged, H-6720 Szeged, Hungary
[4] Wigner Research Centre for Physics of the Hungarian Academy of Science, H-1121 Budapest, Hungary

E-mail: ropagnol@emt.inrs.ca

Keywords: terahertz (THz), far-infrared, intense radiation, nonlinear, semiconductor, antennas, spectroscopy

Abstract

The characteristics of terahertz (THz) radiation generated from large-aperture photoconductive antennas (LAPCAs) were investigated. The antennas were fabricated using different wide-bandgap semiconductor crystals (ZnSe, GaN, 6H–SiC, 4H–SiC and β–Ga_2O_3) as the substrate. We used an amplified sub-picosecond KrF excimer laser for illumination of the LAPCAs. THz emission scaling was studied as a function of the bias field and the pump laser energy. It was found that the radiated THz energy scales quadratically as a function of the bias field and sub-linearly as a function of the optical fluence for most of the substrates. Further, we demonstrate that SiC, and especially 4H–SiC LAPCAs offer the best THz generation performances. In order to generate intense THz radiation, we fabricated both 6H- and 4H–SiC LAPCAs with an interdigitated structure. From the field autocorrelation trace, it was found that the spectra lie in the sub-THz regime, extending up to 400 GHz, with a peak frequency at 50 GHz, making the bridge between the microwaves band and the THz band. The maximum generated THz energy was 11 μJ, which is to date the highest THz energy measured from LAPCA sources, with a corresponding peak electric field of 115 kV cm^{-1} and a corresponding ponderomotive potential of 60 eV. Nonlinear THz experiments were performed using these energetic THz pulses, and open aperture Z-scan experiments in an n-doped InGaAs layer revealed a transmission enhancement of 1.7. It was also shown that in order to have efficient THz generation, the energy contrast of the laser must be kept high.

1. Introduction

Over the last 20 years, terahertz (THz) technology has witnessed great advances and development, opening the window to a wide range of new applications, such as imaging, non-destructive testing, telecommunication and even biologic applications [1–5]. These applications require powerful THz sources with high signal-to-noise ratios. In parallel, thanks to the progress that has occurred with amplified ultrafast lasers, intense table-top THz sources are starting to become widely available as well [6]. The first intense THz source was reported in 1992 by You *et al*, and was a GaAs large-aperture photoconductive antenna (LAPCA) that generated THz pulses with 0.8 μJ energy and a THz peak electric field of 150 kV cm^{-1}, with a peak power of 1.6 MW [7]. After a long period of related inactivity, it was only in 2007 that intense table-top THz sources saw new development, when Blanchard *et al* generated intense THz pulses from a large-aperture ZnTe crystal pumped by an amplified Ti: sapphire laser [8], demonstrating THz pulses with 1.5 μJ energy and a peak THz electric field of 200 kV cm^{-1}, with a peak power of 1.9 MW. In the same year, Yeh *et al* demonstrated the generation of THz pulses with 10 μJ energy, with a THz peak electric field of 250 kV cm^{-1} and a peak power of 5 MW, from a $LiNbO_3$ crystal pumped

by a 10 Hz repetition rate Ti:sapphire laser, using the pulse-front-tilt technique [9]. Today, the $LiNbO_3$ source can generate pulses in the sub-mJ level [10, 11]. It is also one of the most popular intense THz sources, and THz pulses with peak fields larger than 1 MV cm^{-1} and a corresponding peak power of 4 MW have been generated using a kHz amplified Ti:sapphire laser [12]. These THz pulses are mono-cycle with the main frequencies ranging from 0.5 to 2 THz. The two-color plasma source is another intense table-top THz source that is widely used by the THz community [6]. This source generates single-cycle THz pulses with a wide spectrum, with the main frequencies reaching 50 THz and higher [13]. Due to the presence of high frequency components, the THz beam can be focused to a very small spot size, which can induce giant THz peak electric fields of up to 8 MV cm^{-1} for a peak power of 12 MW [14]. Today, more options are studied for the generation of intense THz pulses, such as the spintronic and liquid emitters [15–17].

The increased availability of such intense table-top THz sources is now attracting great interest from the scientific community on their applications, and especially on the nonlinear nonresonant control of matter [7, 18]. For example, single-cycle high-field THz pulses have been used to modify the magnetic structure of multiferroic compounds, such as $TbMnO_3$, by modulating the amplitude of spin-cycloid plane rotation [19], to induce the insulator-to-metal transitions in VO_2 [20], to orient molecules [21] and to disassemble DNA [22]. Other nonlinear effects, such as impact ionization [23], ionization of atoms in gas and solids [24, 25]and field emission [26, 27], have also been demonstrated at THz frequencies. InGaAs is a material that has received considerable attention because of its high carrier mobility and the non-parabolicity of its conduction band [28–34]. Many of these studies have found that when the n-doped InGaAs layer is pumped by an intense THz pulse with fields higher than 100 kV cm^{-1}, absorption bleaching is observed. This is caused by electrons that are accelerated with enough kinetic energy by the THz electric field, resulting in their scattering from the gamma (Γ) valley to the satellite valleys. The electron mobility in these satellite valleys is lower, leading to a drop in conductivity and enhancement of THz transmission. Such phenomena can be used for nonlinear THz imaging, which is especially efficient when using low THz frequencies [34]. Also, an interesting comparison can be made between two experimental observations by Razzari *et al* [28] and Xin *et al* [31], on nonlinear THz optics using THz pulses with the same peak field, but at different central frequencies. They both used intense THz pulses with peak electric fields of around 200 kV cm^{-1}, to irradiate a thin film of n-doped InGaAs with the same characteristics. However, Razzari *et al* used THz pulses with frequencies centered at 1 THz, generated by optical rectification in a large aperture ZnTe crystal [28], while Chai *et al* used those centered at 0.15 THz generated by ZnSe interdigitated LAPCA (ILAPCA) [31]. In these experiments, while Razzari *et al* only observed THz absorption bleaching, Chai *et al* observed significant modulations of the THz waveform, leading to the generation of high frequency components. This high frequency generation resulted from the truncation of the photocurrent induced by the scattering of electrons into the satellite valley, which occurs at timescales that are shorter than the duration of a half-cycle of the pulse. It should be noted that even when the InGaAs layer was strongly pumped by THz pulses with peak field over 1 MV cm^{-1} and centered at 1.5 THz, no variation in the THz spectrums was observed, despite impact ionization being induced [32].

From this example, we see that different characteristics of the intense THz pulses (for example, frequency components and waveform) may lead to different nonlinear THz phenomena. As mentioned above, LAPCAs are the first tabletop sources of intense THz radiation. LAPCAs are also unique THz sources that cover the lower part of the THz spectrum ranging from 0.1 up to 1 THz efficiently. These low frequencies are ideally suited for generating high ponderomotive potential, which can accelerate electrons efficiently [18, 30]. Another uniqueness is the temporal waveform of the radiated pulse itself, since it is quasi half-cycle in nature with high asymmetry, which can impart a non-zero transverse momentum to charged particles because they are not decelerated by an equal, but opposite polarity swing in the field associated with a full-cycle of radiation [35]. However, to date, LAPCAs have not found widespread use as intense THz field sources, since they have traditionally been limited by various technical factors, including their thermal instability, a lack of reliability in terms of premature failures, and saturation of the THz electric field and peak power at relatively low pump laser fluence, thus requiring excessively large apertures [30].

Earlier researches work on LAPCAs to generate THz pulses with intense THz fields by working with an interdigitated structure. This structure allows to reduce the gap size between electrodes while keeping a large aperture for THz output [36]. Using this approach and an LT-GaAs substrate with a 5 μm gap size, THz pulses with a peak field of 36 kV cm^{-1} were generated with an efficiency of 2×10^{-3} [37]. Plasmonic gratings and nanoantennas are another approach that have been tested [38–40]. These specific structures increase light absorption and reduces the average photo-carrier transport path, allowing the collection of a larger number of carriers on a sub-picosecond time scale, thus increasing quantum efficiency. Plasmonic electrodes on a GaAs LAPCA with an interdigitated structure were tested on a 1 mm^2 area and the optical-to-THz conversion efficiency was demonstrated to be 1.6% [41]. Despite these impressive results, these nano- and micro-scale structures are extremely difficult to fabricate on very large areas (~cm dimensions), which would be necessary to generate intense THz pulses with MV cm^{-1} focused fields.

Table 1. Basic physical properties of wide band gap semiconductor crystal tested for the generation of THz radiation from LAPCAs (BFOM is Baliga figure of merit and is used for power and high voltage devices) [47].

Semi-conductor	ZnSe	GaN	6H–SiC	4H–SiC	β–Ga_2O_3
Band-gap (eV)	2.7	3.28	3.01	3.23	4.84
Direct/indirect	D	D	I	I	I/D
Dielectric strength (MV cm^{-1})	1	4	3	3	8
Carrier mobility (cm^2 V^{-1} s^{-1})	500	1000	400	800	300
BFOM	0.5	62	10.4	21	152
Maximum size	6 inches (polycrystalline)	4 inches (high dislocation density)	6 inches	6 inches	15 × 10 mm

Another approach for increasing the peak electric field of THz pulses from LAPCAs is to use semiconductor substrates with wide bandgaps. Indeed, the electric field is linearly proportional to the applied bias field [42]. Wide-bandgap semiconductor crystals have large dielectric strength, which is advantageous, especially in comparison with smaller bandgap semiconductors (such as GaAs), since high bias fields need to be applied to LAPCAs for the generation of high-field THz pulses. Previously, diamond, ZnO, GaN, ZnSe, 4H–SiC and 6H–SiC crystals were tested as substrates for photoconductive antennas [43–46]. Despite showing promising results, most of these substrates have not been tested on a very large aperture for the generation of THz pulses with μJ energy level. One wide-bandgap semiconductor that has been widely studied for LAPCA is ZnSe. While ZnSe (with a bandgap of 2.7 eV) can be pumped below the bandgap via two photon absorption using an 800 nm laser beam, it offers higher performances when pumped above the bandgap using the second harmonic of a Ti: sapphire laser [45]. Using a ZnSe ILAPCA pumped with a 15 mJ, 400 nm laser beam and 60 fs duration, THz pulses with 8 μJ and 14 MW peak power have been generated [30]. Although these studies show promising results, there have been no direct comparisons of their performances. Further, most of these crystals have bandgaps greater than 3.1 eV, which makes the performances of LAPCAs inefficient when pumped with the second harmonic of a Ti:sapphire laser (400 nm laser wavelength).

In this work, we will first study THz generation from ZnSe, GaN, 6H–SiC, 4H–SiC and β–Ga_2O_3 LAPCAs pumped above the bandgap by sub-picosecond KrF laser pulses at 248 nm, and compare their performances. We demonstrate that the scaling of the THz energy as a function of the bias electric field and the optical fluence follow the theory of the current surge model. Further, we show that SiC, and specifically 4H–SiC substrates, offer the best performances. Next, we generate intense THz pulses with high energy output, up to 11 μJ, from 4H–SiC ILAPCAs. From field autocorrelation measurements, we find that the peak frequency is located at 50 GHz, with the spectrum extending up to 400 GHz. The calculated electric field is estimated to be 115 kV cm^{-1}, the peak power 3.6 MW and the ponderomotive potential 60 eV. We demonstrate nonlinear effects using these high-intensity THz pulses by performing Z-scan experiments in an n-doped InGaAs layer, inducing absorption bleaching with a nonlinear transmission enhancement of 1.7.

2. Semiconductor crystals and experimental set up

For these studies, we used ZnSe, GaN, 6H–SiC, 4H–SiC and β–Ga_2O_3 wide bandgap semiconductor crystals as the substrate of the LAPCAs. For each semiconductor, table 1 summarizes the main important characteristics for THz generation from LAPCAs.

From table 1, we can see that all of these crystals have large bandgap and large dielectric strengths (>1 MV cm^{-1}), with the largest being for β–Ga_2O_3 (8 MV cm^{-1}). Further, their carrier mobilities are relatively high (>300 cm^2 V^{-1} s^{-1}), with the highest seen for the GaN crystal. The Baliga figure of merit (BFOM), which is used to characterize materials for power devices for high-frequency applications, is linearly proportional to the dielectric constant, the carrier mobility, and is proportional to the cube of the breakdown field [47]. Obviously, the highest BFOM is obtained for the β–Ga_2O_3 crystal, which takes advantage of its very large breakdown field, and is followed by GaN and 4H–SiC. In terms of bandgap, there are two types of semiconductors: (i) direct bandgap (such as ZnSe and GaN) and (ii) Indirect bandgap (such as 6H–SiC and 4H–SiC). β–Ga_2O_3 is a different case, where the indirect bandgap is 4.84 eV [48] and the direct bandgap at the Γ point is only 0.04 eV higher with a value of 4.88 eV. In this work, since we are pumping our PCAs at a wavelength of 248 nm (5.0 eV), the electrons will be pumped directly into the Γ valley, and β–Ga_2O_3 should be considered as a direct bandgap semiconductor. The last important parameter is the maximum size of the crystal that can be grown. We see from table 1 that ZnSe, GaN, 6H–SiC and 4H–SiC are commercially available with $\geqslant$4 inch size, but for β–Ga_2O_3, the current limit of the substrate size is 15 × 10 mm. Since the output THz energy scales with the area of the LAPCA, this could represent a drawback for generating intense THz pulses from β–Ga_2O_3 LAPCAs.

In the present work, we performed two studies. The first was dedicated to studying and comparing the different performances of LAPCAs fabricated with different semiconductors crystals. In this study, we used a hybrid dye-excimer laser-system (KrF) as the pump laser [49]. The cascade of dye-lasers produces nearly Gaussian seed pulses at 497 nm, with a 500 fs duration. Before amplification, the second harmonic of the seed pulse is generated using a BBO crystal. After amplification, the laser output has a wavelength of 248 nm, a 500 fs duration and energy up to 30 mJ with a beam size of 2 × 2.5 cm. The LAPCAs used in this first study had a simple design, with two 15 mm long and 1 mm wide stripline electrodes with 3 mm gap size. They were fabricated with Cr/Al by sputtering. In the second study, we built 6H–SiC and 4H–SiC ILAPCAs with Cr/Al electrodes, a 1 mm gap size and 40 × 60 mm size, fabricated using the standard photolithography technique. The number of interdigitated electrodes is 20. Therefore, the number of illuminated antennas was 10, since we use a shadow mask to avoid destructive interference from the neighboring antennas. The 248 nm pump beam illuminates an active area of 5.1 cm^2 of the LAPCA. In order to efficiently illuminate the ILAPCA, we used a six-pass amplification laser system, and generated laser pulses with up to 80 mJ of energy and a 700 fs duration. The beam size was 45 × 50 mm, with an estimated 90% of the total area of the ILAPCA illuminated.

Since the laser wavelength was 248 nm, it was not possible to perform electro-optic sampling. To measure the THz energy, we used a pyroelectric detector (Gentec model THz 5I-BL-BNC), with a sensitivity of 78 kV W^{-1} at 0.6 μm wavelength according to the manufacturer's specifications. However, the calibration of the response in the THz frequency range was carried out by cross-calibration with a Coherent-Molectron pyroelectric detector, which was previously calibrated in the THz frequency range. This calibration gave a THz sensitivity of 0.87 V μJ^{-1} for the pyroelectric detector used in this experiment, for a repetition rate lower than 10 Hz. We used two pulsed high-voltage sources for biasing the LAPCAs. The first one was generating voltage pulse up to 6 kV and was used for experiment in air and the second one generates voltage pulse up to 40 kV and was used for experiment in vacuum.

3. Experimental results and discussion

3.1. Performances of LAPCAs made with different substrate

For this first study, we used 15 mm long LAPCAs with a 3 mm gap size. Figure 1(a) shows the experimental configuration, where we used an off-axis parabolic mirror with a 2 inch diameter and a 2 inch focal length for focusing the THz beam onto the pyroelectric detector. Figures 1(b) and (c) show the scaling of the THz energy for the different LAPCAs (fabricated using ZnSe, GaN, 6H–SiC, 4H–SiC and β–Ga_2O_3) as a function of the bias field and optical fluence, respectively. Figure 1(d) shows the square root scaling of the THz energy, which is proportional to the THz electric field, as a function of optical fluence. The dots represent the experimental results, and the lines, the fitting. First, we can see that the different substrates offer different performances. The most efficient LAPCAs are 4H–SiC, followed by 6H–SiC, GaN, β–Ga_2O_3 and ZnSe. For example, when the LAPCAs are biased at 18 kV cm^{-1}, the 4H–SiC LAPCA is 50% and 100% more efficient than the 6H–SiC and the GaN LAPCAs, respectively. We also observe that for all substrates, the THz energy scales quadratically as a function of the bias field, which is expected from theory. The fitting curves in figure 1(b) confirm the quadratic scaling. The maximum bias field was limited by the high voltage source itself, and not by the substrate. Conversely, the scaling of the THz energy as a function of optical fluence is sublinear, and by plotting the square root of the THz energy as a function of optical fluence, we can see the onset of saturation. This saturation is also expected, and is the consequence of THz radiation screening. In principle, the THz electric field has a hyperbolic behavior and is proportional to [50]:

$$\sqrt{W_{\mathrm{THz}}} \propto \beta\left(\frac{F}{F + F_{\mathrm{sat}}}\right). \tag{1}$$

Here, W_{THz} is the THz energy, F is the optical fluence and F_{sat} is the saturation fluence, which corresponds to the fluence needed for extracting half of the maximum radiated THz field and is defined by [51]:

$$F_{\mathrm{sat}} = \frac{h\nu(1 + \sqrt{\varepsilon})}{e\mu\eta_0(1 - R)}. \tag{2}$$

Here, $h\upsilon$ is the photon energy, ε is the dielectric constant, e is the electron charge, μ is the electron mobility, η_0 is the free impedance and R is the reflectivity of the substrate at the excitation wavelength. We find that while the THz energy radiated from most substrates shows a hyperbolic behavior, the GaN LAPCA does not. Table 2 summarizes the parameters obtained from the fitting curves, F_{sat} and μ for all the substrates except GaN:

In table 2, the saturation fluence ranges from 1.39 mJ cm^{-2}, for β–Ga_2O_3, to 1.06 mJ cm^{-2}, for ZnSe. However, considering the error bar, we can conclude that all the saturation fluences are in the same range. The saturation fluences of the ZnSe and 6H–SiC LAPCA pumped with 248 nm laser is around 5 times larger than

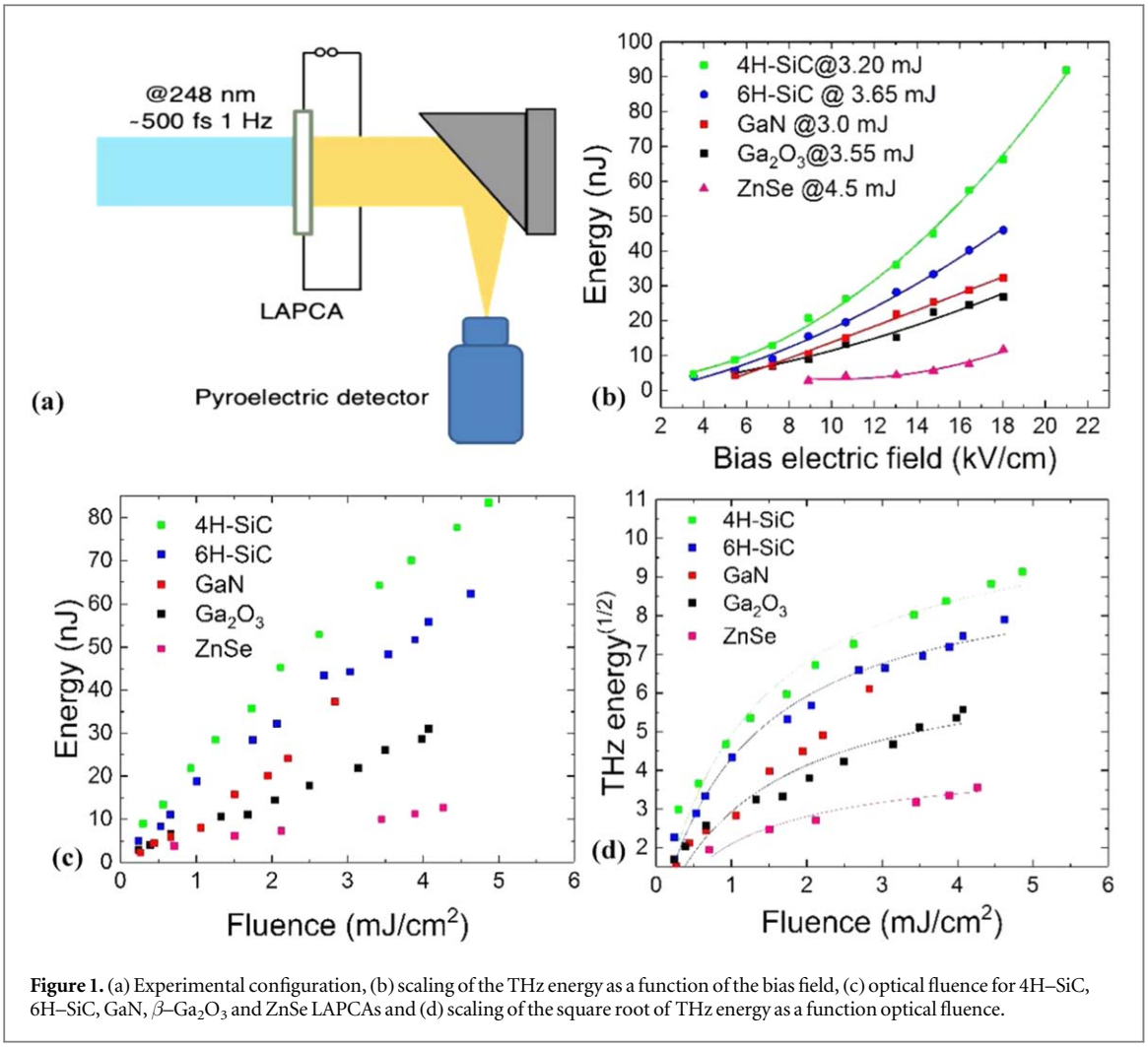

Figure 1. (a) Experimental configuration, (b) scaling of the THz energy as a function of the bias field, (c) optical fluence for 4H–SiC, 6H–SiC, GaN, β–Ga_2O_3 and ZnSe LAPCAs and (d) scaling of the square root of THz energy as a function optical fluence.

Table 2. Fitting parameters F_{sat} and calculated μ obtained from the experimental results located in figure 1(d).

	ZnSe	GaN	6H–SiC	4H–SiC	β–Ga_2O_3
F_{sat}(mJ cm^{-2})	1.06 ± 0.18	—	1.20 ± 0.14	1.24 ± 0.16	1.39 ± 0.25
μ (cm^2 V^{-1} s^{-1})	52 ± 9	—	63 ± 8	61 ± 8	55 ± 12

when they are pumped with 400 nm femtosecond laser [46, 51]. Using equation (2), we calculate the transient carrier mobility, and find a transient mobility ranging from 52 cm^2 V^{-1} s^{-1}, for ZnSe, to 63 cm^2 V^{-1} s^{-1} for 6H–SiC. Although the initial carrier mobility shows a large difference between the different substrates, the transient mobility shows a smaller variation. Further, the transient mobilities of ZnSe and 6H–SiC—when pumped by the 248 nm laser—are 3.8 and 2.8 times smaller than the transient mobilities when pumped by 400 nm laser, respectively. The main reason for this difference is that when pumping with the 248 nm laser, the photon energy is much larger than the bandgap of the different substrates, except for β–Ga_2O_3. This results in the carriers being pumped directly into the higher valleys, where their effective mass is higher and the electron mobility lower. The difference in saturation fluence, and more specifically, the difference in transient mobility, cannot fully explain the difference in the performances of the LAPCAs. We believe that when lasers with high photon energies are used to pump the LAPCA, the inter- and intra-valley carrier dynamics are much more significant. Unfortunately, since we were not able to measure the radiated THz waveform, we do not have enough information to come up with a detailed explanation of the inter- and intra-valley carrier dynamics involved [52].

3.2. Interdigitated large aperture photoconductive antennas

For the generation of intense THz pulses, we fabricated ILAPCAs using 6H–SiC and 4H–SiC wafers. Figure 2(a) shows a picture of the ILAPCA deposited on a 4 inch diameter wafer and the shadow mask deposited on a quartz

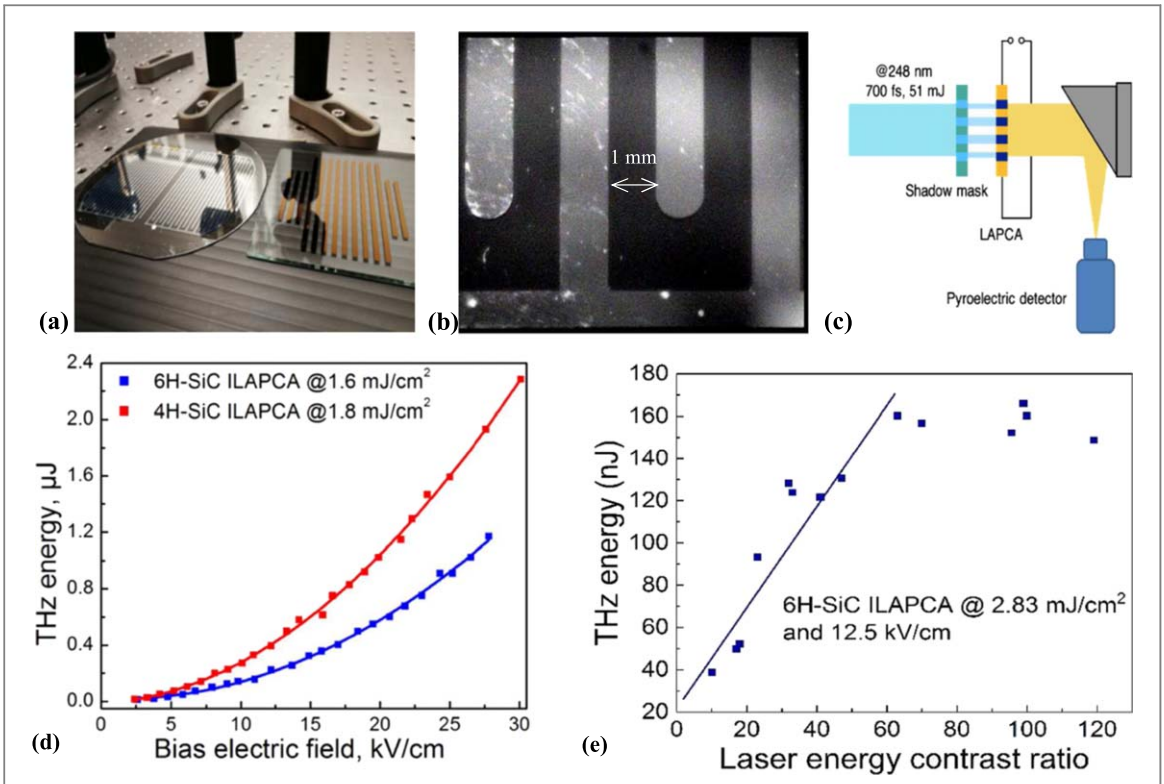

Figure 2. (a) Photo of the structure of two ILAPCAs on a 4 inch diameter 6H–SiC wafer and the shadow mask, (b)microscope image of the rounding edge of the ILAPCA structure on the 4H–SiC substrate, (c) scheme of the experimental set-up, (d) scaling of the THz energy as a function of bias electric field for 6H–SiC and 4H–SiC ILAPCAs, and (e) scaling of the THz energy as a function of the laser energy contrast ratio for the 6H–SiC ILAPCA biased at 12.5 kV cm^{-1} and pumped with 2.83 mJ cm^{-2}.

window. Figure 2(b) is a schematic diagram of the experimental setup, figure 2(c) shows the scaling of the THz energy as a function of the bias field when the 6H–SiC and 4H–SiC ILAPCAs are pumped with pump laser fluences of 1.55 and 1.82 mJ cm^{-2} in air, and figure 2(d) shows the influence of the laser contrast ratio on the THz energy for the 6H–SiC ILAPCAs biased at 12.5 kV cm^{-1} and pumped with 2.83 mJ cm^{-2} with a 2.6 cm diameter beam.

The scaling of the THz pulse energy radiated by the 6H–SiC and the 4H–SiC LAPCAs as a function of bias field is quadratic. We can also see that the 4H–SiC ILAPCA offers better performance than the 6H–SiC ILAPCA, which is consistent with the result shown in figure 1(b). At an 18 kV cm^{-1} bias field, the 4H–SiC ILAPCAs is 70% more efficient than the 6H–SiC LAPCA. However, at 27 kV cm^{-1}, the 4H–SiC is twice as efficient as the 6H-ILAPCAs. In these experiments, the maximum bias field was limited by the air breakdown and not by the breakdown of the substrate itself. At the maximum bias field in air of 30 kV cm^{-1}, the energy of the THz pulse generated by the 4H–SiC LAPCA is 2.3 μJ. Another point that we noticed was that after we filled out the KrF laser with a fresh gas, we usually had a drop in the THz energy, although other experimental conditions were kept the same. This is due to changes in the laser energy contrast ratio. After the chamber of the laser is filled with new gas, the laser energy contrast-ratio drops due to the strong amplified spontaneous emission (ASE) of the pulse [53]. Here, the energy contrast ratio is defined as the ratio of the energy contained in the pedestal to the total energy of the laser pulse. By putting an attenuator just before the entrance of the last amplification stage, we were able to increase the energy contrast ratio from 10 to above 100. From figure 2(d), we can see that the THz energy scales almost linearly with energy contrast ratio up to 60 before reaching a plateau. In the case of the KrF laser, the ASE has a 10 ns duration, starting 7.5 ns before the main pulse. Note that due to the poor focusability and long duration of the ASE, the intensity contrast can be high even if the energy contrast is low. In our case, however, the beam was kept parallel, and thus the energy contrast was critical. The main reason for the drop in the THz energy when the laser contrast ratio is low is that the pre-pulse excites electrons into the conduction band. If the density of electrons generated by the pre-pulse is too high, the LAPCAs will switch before the arrival of the main pulse. In this case, when the main pulse illuminates the LAPCA, the switch is still in the 'On'-state, which strongly decrease the generation of THz waves. Consequently, in all the experiments dealing with the ILAPCAs, we ensure that the energy contrast ratio of the laser is over 60.

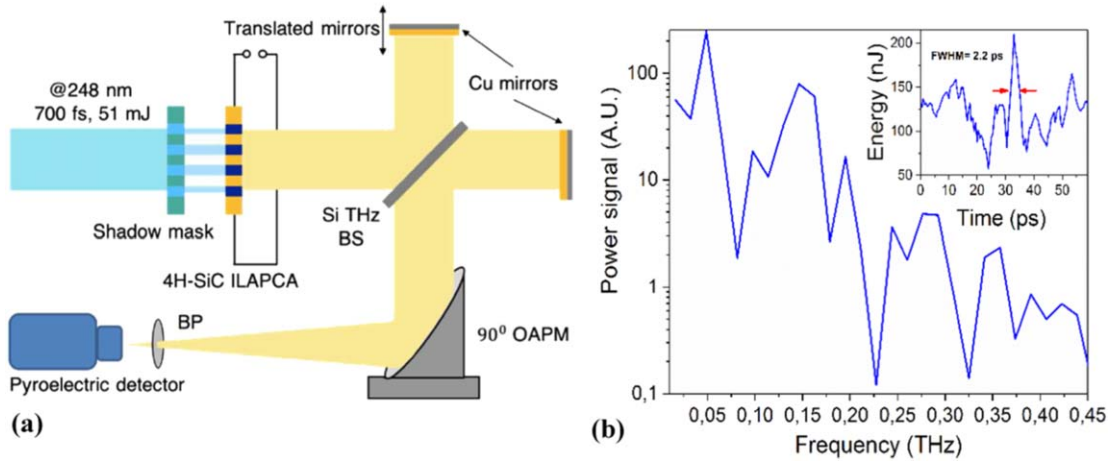

Figure 3. (a) Scheme of the THz Michelson interferometer (Si BS: Silicon beam splitter, 90° OAPM: 90° off axis parabolic mirror, BP: Black polyethylene). (b) THz spectrum obtained by FFT.

3.3. Interferometric measurement

The KrF laser has a variable repetition rate of up to 10 Hz. It has been demonstrated that standard electro-optic sampling of THz radiation from LAPCAs is possible even at a 10 Hz repetition rate [30]. However, in this particular case, the short wavelength of the KrF laser (248 nm) significantly complicates the choice of the electro-optic crystal. As a result, we did not perform electro-optic sampling detection. Nevertheless, it is important to measure the spectral information and to that end, we built a Michelson THz interferometer to measure the field autocorrelation trace of the THz pulse. Figure 3(a) shows the scheme of the experimental set-up and figure 3(b) the THz spectrum, for a 4H–SiC ILAPCA THz emitter with a bias field of 25 kV cm^{-1} and an optical fluence of 2.3 mJ cm^{-2}. The inset shows the interferometric trace.

From this interferometric trace, we find that, taking into account the 1.4 factor for a Gaussian pulse, the full width at half maximum (FWHM) temporal duration, which is also the duration of the half-cycle, is 2.2 ps. This duration is 4 times longer than the FWHM temporal duration of the half-cycle THz pulse generated by ZnSe ILAPCAs pumped by a 400 nm laser pulse [30]. The main reason for this difference can be explained by the longer duration of the KrF laser used in this experiment. The longer duration of the THz pulse generates lower frequencies that are located at sub-THz frequencies. As can be seen from figure 3(b), the THz frequency extends up to 400 GHz with a peak frequency located at 50 GHz. We also note the presence of multiple echoes in the time domain, which is due to the reflection of the THz pulse at the interface between the 4H–SiC substrate and air, and the Si wafer and air, which also results in the multiple dips within the THz spectrum.

3.4. Nonlinear interaction

Next, we generated THz pulses with the highest intensity possible and studied their nonlinear interaction with an n-doped semiconductor. We placed the 4H–SiC ILAPCA in a vacuum chamber. Figure 4(a) shows the experimental set up. The maximum bias field we could apply before Corona discharges appeared was 64 kV cm^{-1} and the optical pump energy was 54 mJ. The energy of the THz pulses was measured to be 11 μJ, which is the highest THz pulse energy generated by LAPCAs to date. We note that the THz spot size was slightly larger than the 5 mm aperture of the pyroelectric detector at the focal position of the first off-axis mirror and the whole energy of the THz pulse was not totally measured.

We calculated the THz peak electric field using equation (3) [7]:

$$E_{\mathrm{THz}}^{\mathrm{peak}} = \sqrt{\frac{2\eta_0 W}{\tau A}}. \tag{3}$$

Here, η_0 is the impedance of free space, τ is the duration of the THz pulse (2.2 ps at FWHM), A is the area of the THz spot size (5 mm diameter) and W is the THz energy (8 μJ after considering the reflection of the THz pulse at the 4H–SiC/air interface). The THz peak electric field is estimated to be 117 kV cm^{-1} and the peak power is 3.6 MW. Although the peak electric field is not that high, it is the ponderomotive potential of these pulses that is extreme with 60 eV. This is almost 6 times higher than the ponderomotive potential of a pulse with a 1 MV cm^{-1} peak electric field at a frequency of 1 THz [18].

In order to demonstrate the intense nature of these pulses, we performed a nonlinear transmission experiment in an n-doped $In_{0.53}Ga_{0.47}As$ sample with Z-scan. The sample was a 500 nm thick n-type $In_{0.53}Ga_{0.47}As$ epilayer with a doping concentration of 2.0 $\times$ 10^{18} cm^{-3}, grown on a lattice-matched 350 μm

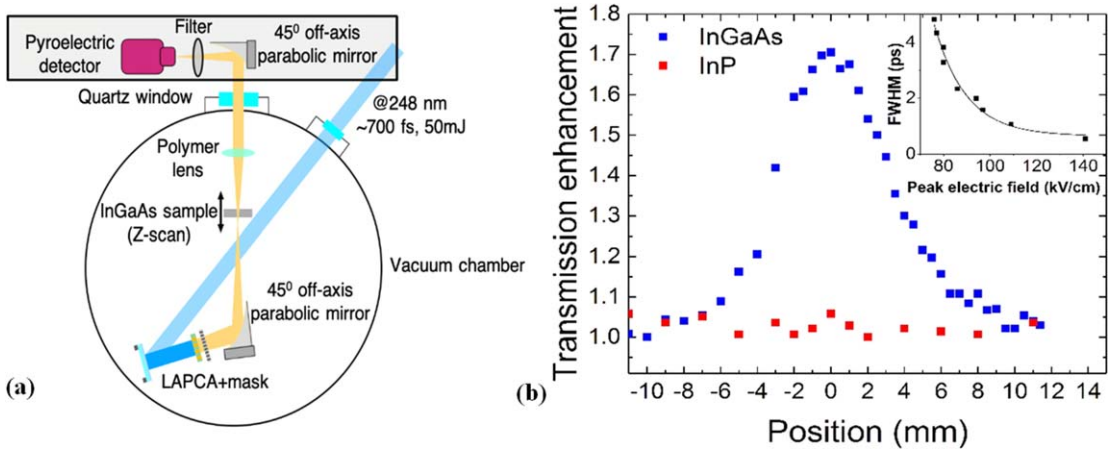

Figure 4. (a): Experimental scheme of the Z-scan experiment with the InGaAs sample and (b) normalized transmission as a function of the Z-scan position for the InGaAs sample and the InP substrate, with a THz pulse energy of 11 μJ. Inset shows the simulated results of the FWHM duration of the THz pulse as a function of the THz peak electric field for a transmission enhancement of 1.7.

thick semi-insulating InP wafer with a dark resistivity higher than $1 \times 10^7\ \Omega$ cm. This $In_{53}Ga_{47}As$ sample is identical to the one that was used in our previous study, as well as in the study by Razzari *et al* [28]. Figure 4(b) shows the normalized transmission enhancement versus the focus position when the THz pulses are transmitted through the InGaAs sample. Note that we do not observe any transmission enhancement when the THz pulse is transmitted through the InP substrate. The maximum transmission enhancement factor observed is 1.7, which is close to what can be obtained with a 200 kV cm^{-1} electric field at a central frequency of 1 THz.

Absorption bleaching inside $In_{53}Ga_{47}As$ can be also used for characterizing the electric field. Here, we used an analytical-band ensemble Monte Carlo approach as a solution of the Boltzmann transport equation, which is identical to the one used in our previous experiment [31], and we simulated the nonlinear transmission enhancement induced by these THz pulses. For the simulations, we assumed the THz waveform to be a half-cycle pulse and we simply varied the duration of the pulse. Then we calculated the nonlinear transmission enhancement, for different electric fields and different FWHM durations. The inset in figure 4(b) shows the evolution of the FHWM duration of the THz pulse as a function of the THz peak electric field for achieving a nonlinear transmission enhancement of 1.7. We can see that for a THz pulse with a duration of 2.2 ps, the predicted THz peak electric field needed to observe a transmission enhancement of 1.7 is 90 kV cm^{-1}, which is comparable with the THz field used in our experiments.

4. Conclusion

To summarize, we studied the performances of different wide bandgap semiconductor LAPCAs (ZnSe, GaN, 6H–SiC, 4H–SiC and β–Ga_2O_3) pumped by an amplified KrF laser at a 248 nm laser wavelength. The experiments demonstrate that the large photon energy of the KrF laser makes it an excellent pumping source for the generation of THz radiation with the photoconductive antenna mechanism. We found that SiC, and especially the 4H–SiC LAPCAs offer the best performances for generating THz waves. Our results show that the saturations fluence of these LAPCAs are relatively high, due mainly to the scattering of electrons into the satellite valley. Additionally, the scaling of the THz energy versus bias field is quadratic, and does not show any sign of saturation, which is an important factor when considering the generation of intense THz waves. We fabricated 6H–SiC and 4H–SiC ILAPCAs for the generation of intense THz pulses. By measuring an interferometric trace of the pulse, we found that the radiated electromagnetic waves had sub-THz frequencies, extending up to 400 GHz and the peak located at 50 GHz. By placing the 4H–SiC ILAPCAs in a vacuum chamber, we were able to generate a THz pulse with an energy of 11 μJ, which is the highest energy that has been generated from a LAPCA to date. The peak electric field was estimated to be 117 kV cm^{-1} with a peak power of 3.6 MW, and a ponderomotive energy of 60 eV. Using these high intensity THz pulses in a Z-scan experiment on an n-doped $In_{53}Ga_{47}As$ crystal, we observed a nonlinear transmission factor of 1.7.

Acknowledgments

The authors gratefully thank LaserlabEurope for their financial support, which offered us the opportunity to perform experiments with the subpicosecond KrF laser located in the Department of Experimental Physics at the University of Szeged.

The research leading to these results received funding from the European Union's Horizon 2020 research and innovation program, under grant agreement no. 654148 Laserlab-Europe and co-financed by the European Social Fund EFOP-3.6.2-16-2017-00005 entitled by Ultrafast physical processes in atoms, molecules, nanostructures and biology structures and the support of the Hungarian Scientific Research Fund OTKA 113222.

The authors would like to emphasize that this work is a collaboration between three different universities located in Hungary and in Canada.

References

[1] Guerboukha H, Nallappan K and Skorobogatiy M 2018 *Adv. Opt. Photonics* **10** 843
[2] Zhuldybina M, Ropagnol X, Trudeau C, Bolduc M, Zednik R J and Blanchard F 2019 *Sensors* **19** 444
[3] Sengupta K, Nagatsuma T and Mittleman D M 2018 *Nat. Electron.* **1** 622–35
[4] Kiwa T, Tenma A, Takahashi S, Sakai K and Tsukada K 2013 *Sensors Actuators* B **187** 8–11
[5] Hassan E M, Mohamed A, DeRosa M C, Willmore W G, Hanaoka Y, Kiwa T and Ozaki T 2019 *Sensors Actuators* B **287** 595–601
[6] Hafez H A, Chai X, Ibrahim A, Mondal S, Férachou D, Ropagnol X and Ozaki T 2016 *J. Opt.* **18** 1–48
[7] You D, Jones R, Bucksbaum P H and Dykaar D R 1993 *Opt. Lett.* **18** 290–2
[8] Blanchard F *et al* 2007 *Opt. Express* **15** 13212–20
[9] Yeh K L, Hoffmann M C, Hebling J and Nelson K A 2007 *Appl. Phys. Lett.* **90** 10–4
[10] Fülöp J A, Ollmann Z, Lombosi C, Skrobol C, Klingebiel S, Pálfalvi L, Krausz F, Karsch S and Hebling J 2014 *Opt. Express* **22** 20155
[11] Fülöp J A, Pálfalvi L, Klingebiel S, Almási G, Krausz F, Karsch S and Hebling J 2012 *Opt. Lett.* **37** 557
[12] Hirori H, Doi A, Blanchard F and Tanaka K 2011 *Appl. Phys. Lett.* **98** 10–2
[13] Oh T I, You Y S, Jhajj N, Rosenthal E W, Milchberg H M and Kim K Y 2013 *New J. Phys.* **15** 075002
[14] Oh T I, Yoo Y J, You Y S and Kim K Y 2014 *Appl. Phys. Lett.* **105** 1–5
[15] Seifert T, Jaiswal S, Sajadi M, Jakob G, Winnerl S, Wolf M, Kläui M and Kampfrath T 2017 *Appl. Phys. Lett.* **110** 252402
[16] Jin Q, Williams K, Yiwen E, Dai J and Zhang X C 2017 *Appl. Phys. Lett.* **111** 071103
[17] Balakin A V, Bunkin A F, Makarov V A, Kotelnikov I A, Kuzechkin N A, Savelev A B, Solyankin P M and Shkurinov A P 2018 *Photonics Res.* **7** 678–86
[18] Kampfrath T, Tanaka K and Nelson K A 2013 *Nat. Photon.* **7** 680–90
[19] Kubacka T *et al* 2014 *Science* **343** 1333–6
[20] Liu M *et al* 2012 *Nature* **487** 345–8
[21] Fleischer S, Zhou Y, Field R W and Nelson K A 2011 *Phys. Rev. Lett.* **107** 163603
[22] Greschner A A, Ropagnol X, Kort M, Zuberi N, Perreault J, Razzari L, Ozaki T and Gauthier M A 2019 *J. Am. Chem. Soc.* **141** 3456–69
[23] Hirori H, Shinokita K, Shirai M, Tani S, Kadoya Y and Tanaka K 2011 *Nat. Commun.* **2** 594–6
[24] Li S and Jones R R 2014 *Phys. Rev. Lett.* **112** 1–5
[25] Mukai Y, Hirori H and Tanaka K 2013 *Phys. Rev.* B **87** 1–4
[26] Iwaszczuk K, Zalkovskij M, Strikwerda A C and Jepsen P U 2015 *Optica* **2** 116
[27] Herink G, Wimmer L and Ropers C 2014 *New J. Phys.* **16** 123005
[28] Razzari L *et al* 2009 *Phys. Rev.* B **79** 3–6
[29] Blanchard F *et al* 2011 *Phys. Rev. Lett.* **107** 1–4
[30] Ropagnol X, Khorasaninejad M, Raeiszadeh M, Safavi-Naeini S, Bouvier M, Côté C Y, Laramée A, Reid M, Gauthier M A and Ozaki T 2016 *Opt. Express* **24** 11299
[31] Chai X, Ropagnol X, Raeis-Zadeh S M, Reid M, Safavi-Naeini S and Ozaki T 2018 *Phys. Rev. Lett.* **121** 143901
[32] Chai X *et al* 2018 *Opt. Lett.* **43** 5463
[33] Rovere A, Jeong Y-G, Piccoli R, Lee S-H, Lee S-C, Kwon O-P, Jazbinsek M, Morandotti R and Razzari L 2018 *Opt. Express* **26** 2509
[34] Blanchard C X, Tanaka T, Arikawa T, Ozaki T, Morandotti R and Tanaka T 2018 *Opt. Lett.* **43** 4997
[35] Fallahi A and Kartner F 2018 *J. Phys. B: At. Mol. Opt. Phys.* **51** 144001–12
[36] Winnerl S 2012 *J. Infrared, Millimeter, Terahertz Waves* **33** 431–54
[37] Beck M, Schäfer H, Klatt G, Demsar J, Winnerl S, Helm M and Dekorsy T 2010 *Opt. Express* **18** 9251
[38] Berry C W, Wang N, Hashemi M R, Unlu M and Jarrahi M 2013 *Nat. Commun.* **4** 1610–22
[39] Lepeshov S, Gorodetsky A, Krasnok A, Rafailov E and Belov P 2017 *Laser Photonics Rev.* **11** 1600199
[40] Lepeshov S, Gorodetsky A, Krasnok A, Toropov N, Vartanyan T A, Belov P, Alú A and Rafailov E U 2018 *Sci. Rep.* **8** 6624
[41] Yardimci N T, Yang S H, Berry C W and Jarrahi M 2015 *IEEE Trans. Terahertz Sci. Technol.* **5** 223–9
[42] Stone M R, Naftaly M, Miles R E, Fletcher J R and Steenson D P 2004 *IEEE Trans. Microw. Theory Tech.* **52** 2420–9
[43] Ono S *et al* 2005 *Appl. Phys. Lett.* **87** 1–3
[44] Imafuji O, Singh B P, Hirose Y, Fukushima Y and Takigawa S 2007 *Appl. Phys. Lett.* **91** 2005–8
[45] Ropagnol X, Morandotti R, Ozaki T and Reid M 2011 *IEEE Photonics J.* **3** 174–86
[46] Ropagnol X, Bouvier M, Reid M and Ozaki T 2014 *J. Appl. Phys.* **116** 043107
[47] Baliga B J 1982 *J. Appl. Phys.* **53** 1759–64
[48] Stepanov S I, Nikolaev V I, Bougrov V E and Romanov A E 2016 *Rev. Adv. Mater. Sci.* **44** 63–86
[49] Szatmári S 1994 *Appl. Phys.* B **58** 211–23
[50] Ropagnol X, Blanchard F, Ozaki T and Reid M 2013 *Appl. Phys. Lett.* **103** 161108
[51] Hattori T, Ukamoto K T and Akatsuka H N 2001 *Appl. Phys.* **40** 4907–12
[52] Loata G C, Thomson M D, Löffler T and Roskos H G 2007 *Appl. Phys. Lett.* **91** 1–4
[53] Földes I B, Kocsis G, Racz E, Szatmari S and Veres G 2003 *Laser Part. Beams* **21** 517–21